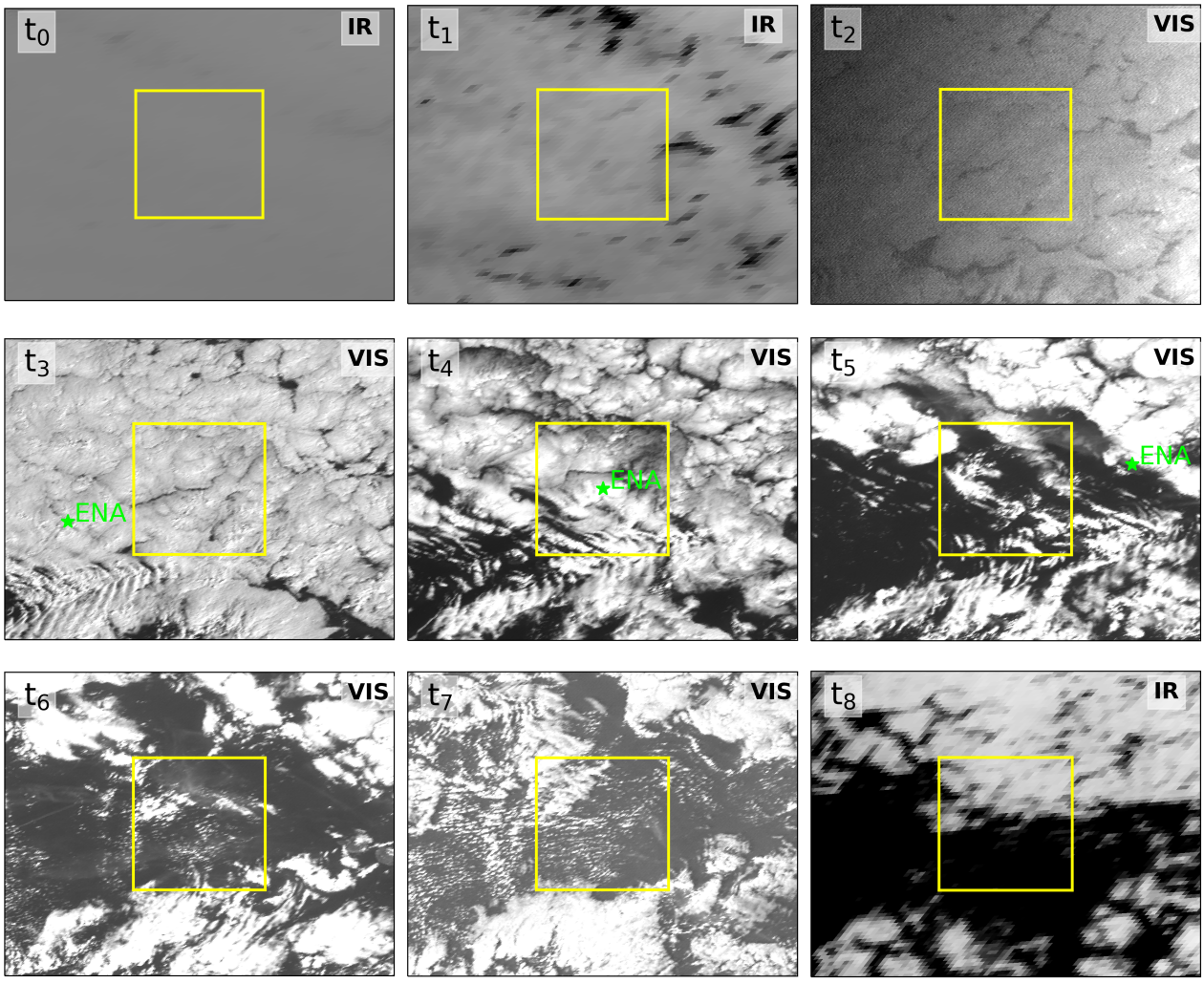

Figure S1. GOES satellite imagery provided for 9 discrete times along the Lagranian trajectory described in Figure 1. Images span two-times the spatial extent of the averaging domain (yellow box) and during the daylight hours visible imagery is shown (0.64-μm reflectance) and at night the infrared imagery (11-μm brightness temperature) is displayed.

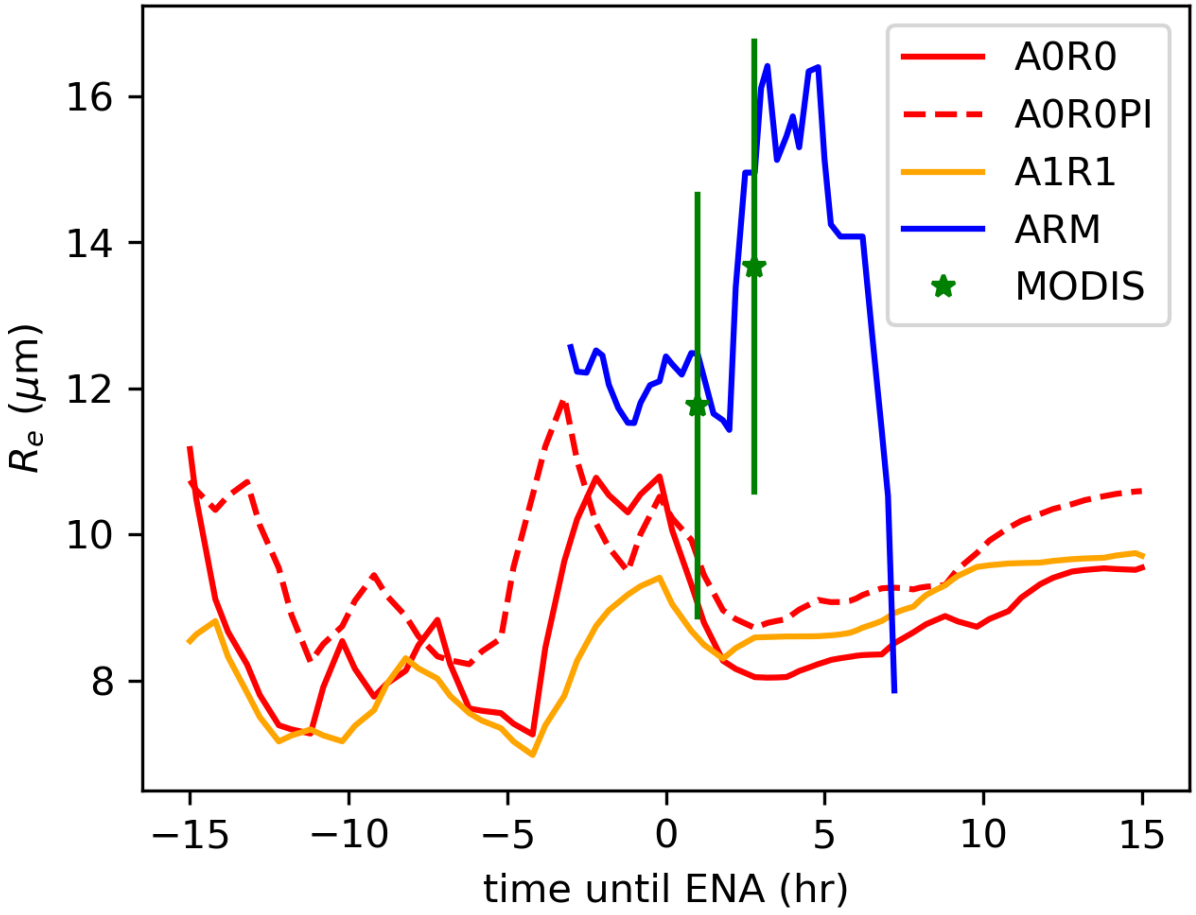

Figure S2. Time series of cloud droplet effective radius at the ARM ENA site for the duration of the lagrangian trajectory for that simulated by the E3SM model under present day (red;solid) and pre-industrial based aerosol emissions (red; dashed) for two different autoconversion and accretion configurations as discussed in Table 2, and retrieved by ARM MSFR (blue) and, MODIS (green). Standard deviations in R_e over the averaging domain of the MODIS data are provided for both Terra (at about hour 1) and Aqua (at about hour 3).

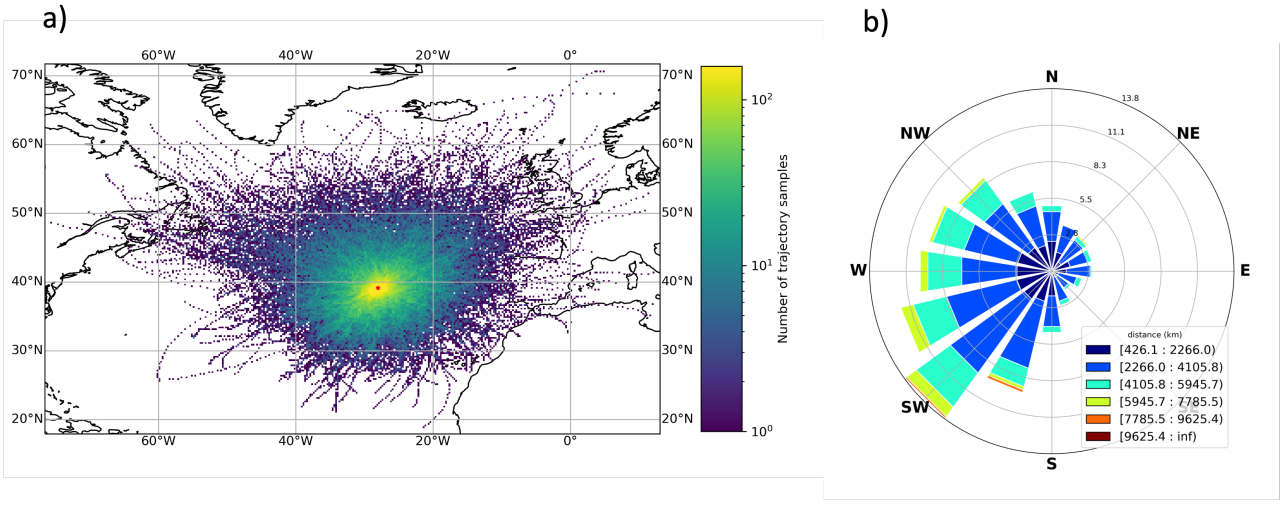

Figure S3. (a) Contour map of the number of hourly samples from trajectories calculated across our region in this study. (b) Wind rose showing the frequency of occurrence of the mean direction of all the trajectories in this study.

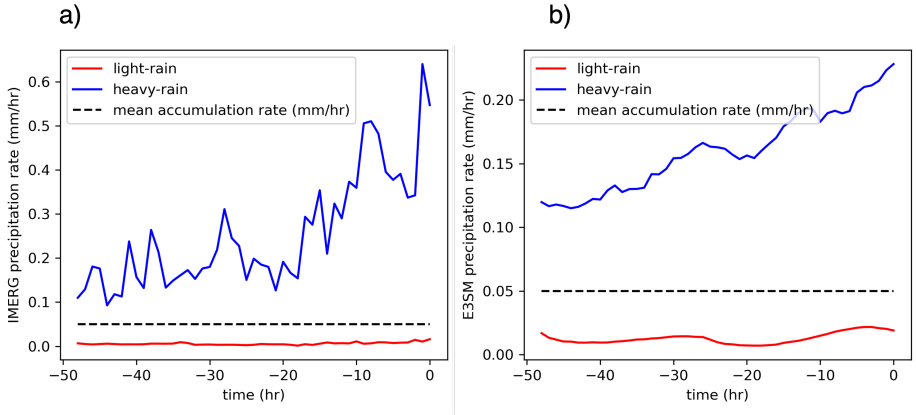

Figure S4. Time series of precipitation rates derived from a Eulerian framework at the ARM ENA site for (a) IMERG and (b) E3SM model for days sorted by above-median (red) and below-median (blue) precipitation rates. Note, the range in precipitation rates (y-axis) differ between data sets.

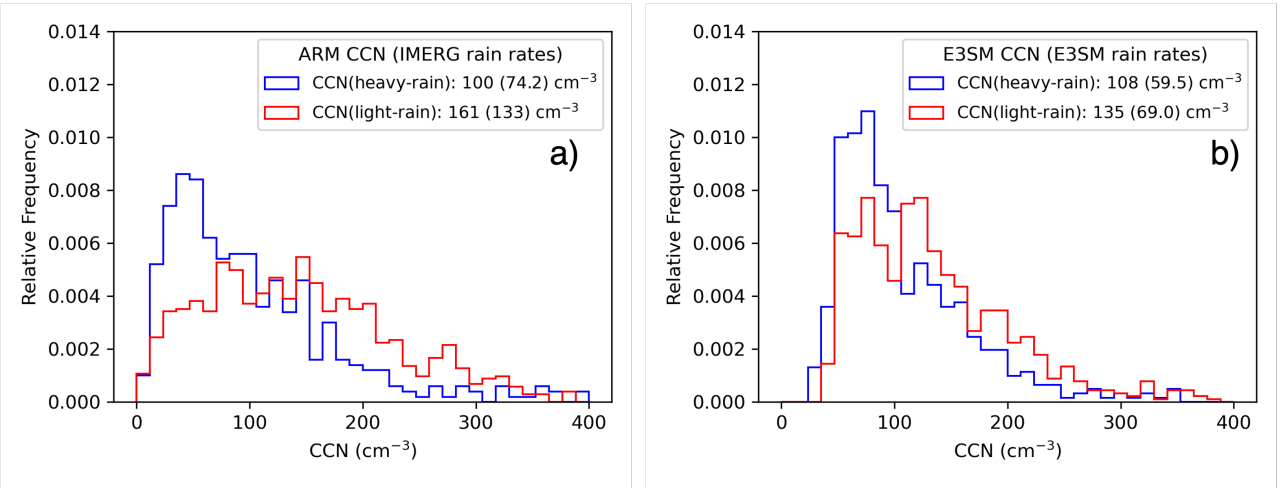

Figure S5. (a) Relative frequency in the distribution of CCN concentration measured at 0.2% supersaturation observed by ARM at the ENA site with above (blue) and below (red) median accumulated IMERG precipitation in the previous 48-hours from the Eulerian perspective. (b) Shows the same distributions from the same trajectories but using E3SM CCN concentration and precipitation rates instead. Means and standard deviations (shown in parenthesis) are provided for each distribution.

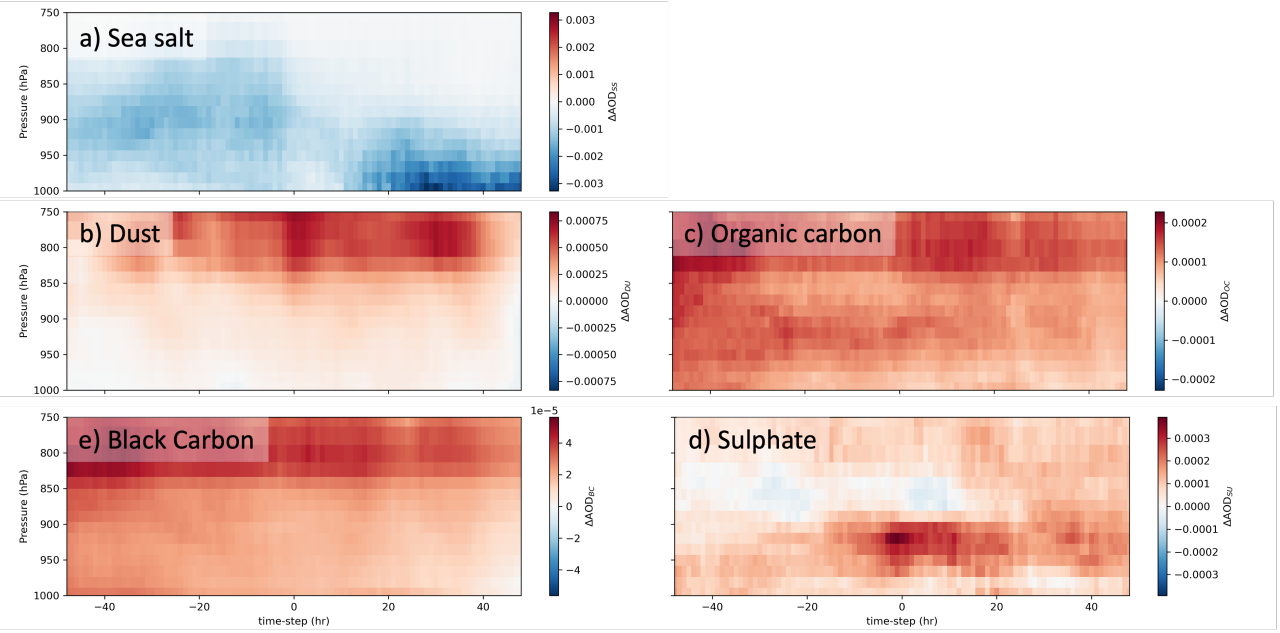

Figure S6. Aerosol optical depth difference between polluted and clean trajectories as determined by the CCN concentration being greater than and less than 110 cm $^{-3}$ at the start of the trajectory decomposed into a) sea salt, b) dust, c) organic matter, d) black carbon, and e) sulfate from MERRA2 averaged into hourly intervals along backward and forward trajectories over the period 06/21/2016 – 08/29/2020. Note, the range of values varies for each subplot according to the maximum range specified on the color bar.

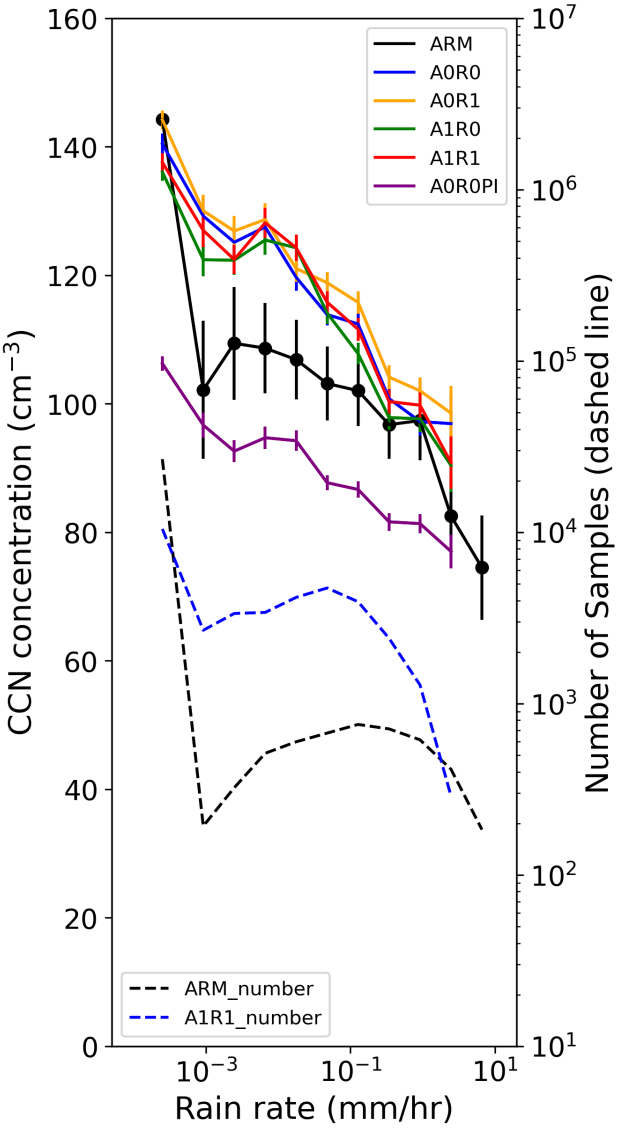

Figure S7. Binned CCN concentration at 0.2% super saturation plotted as a function of hourly rain rate (solid lines) for ARM and each E3SM simulation experiment from the ENA site over the analysis period. Number of samples in each bin are included (dashed lines) along with the 5-95% confidence intervals on CCN concentration for each rain rate bin. Note, the first bin can include non-precipitating clouds.

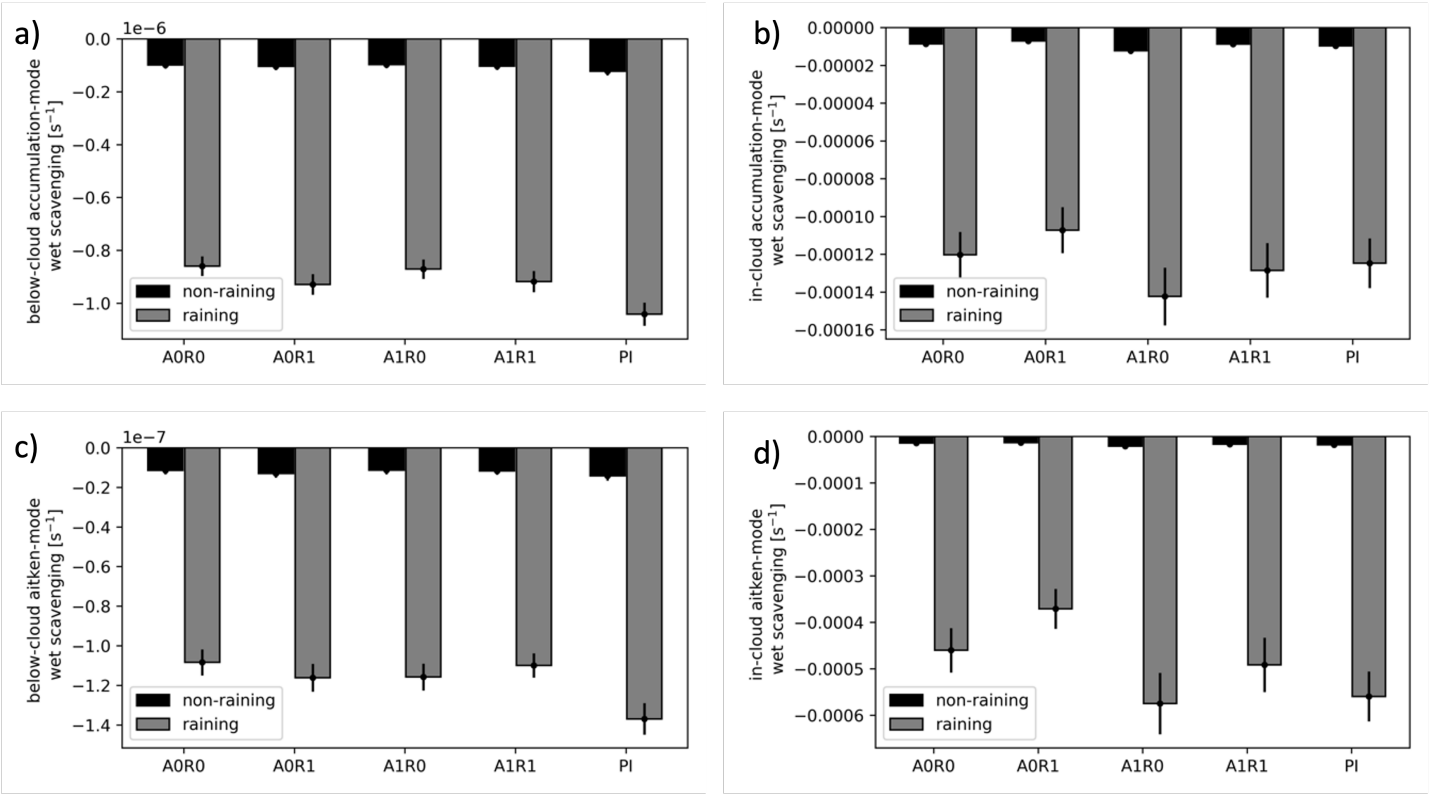

Figure S8. Mean wet scavenging rates for below- (a, and c) and in-cloud (b and d) accumulation-mode aerosols separated by trajectories with below (black; non-raining) and above (gray; raining) median precipitation rates at Graciosa Island shown for each sensitivity experiment (A0R0, A0R1, A1R1, A1R1, PI).

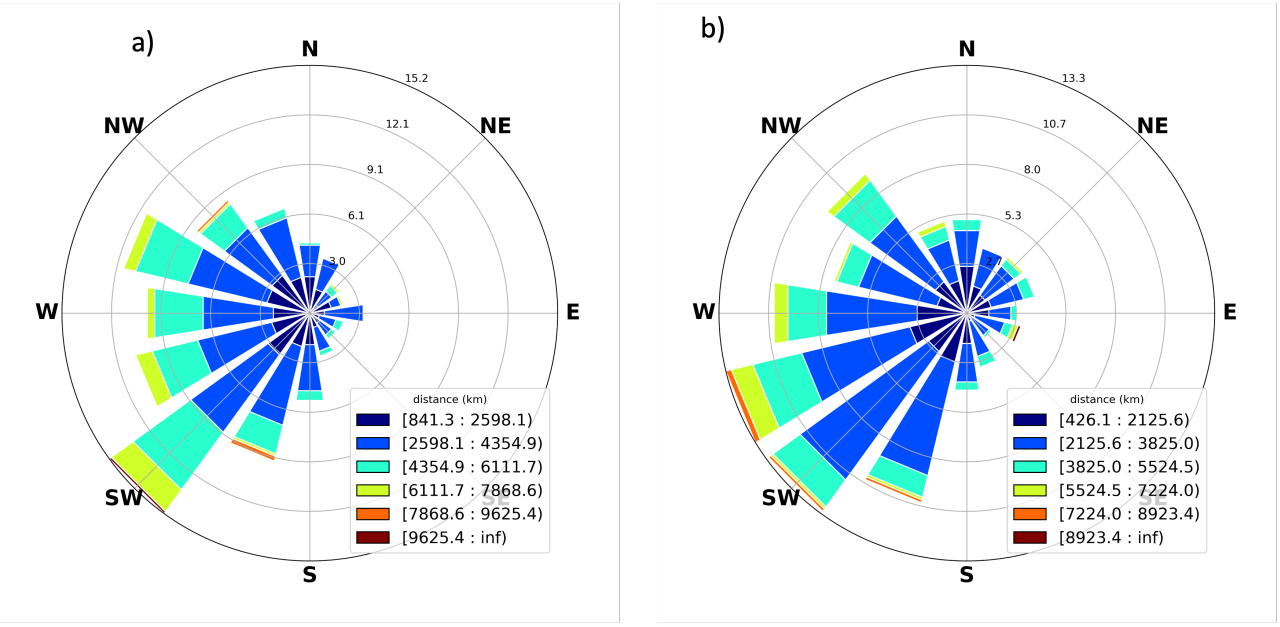

Figure S9. Wind rose showing the frequency of occurrence of the mean direction of the clean (a) and (b) polluted trajectories sorted by CCN concentration in this study.

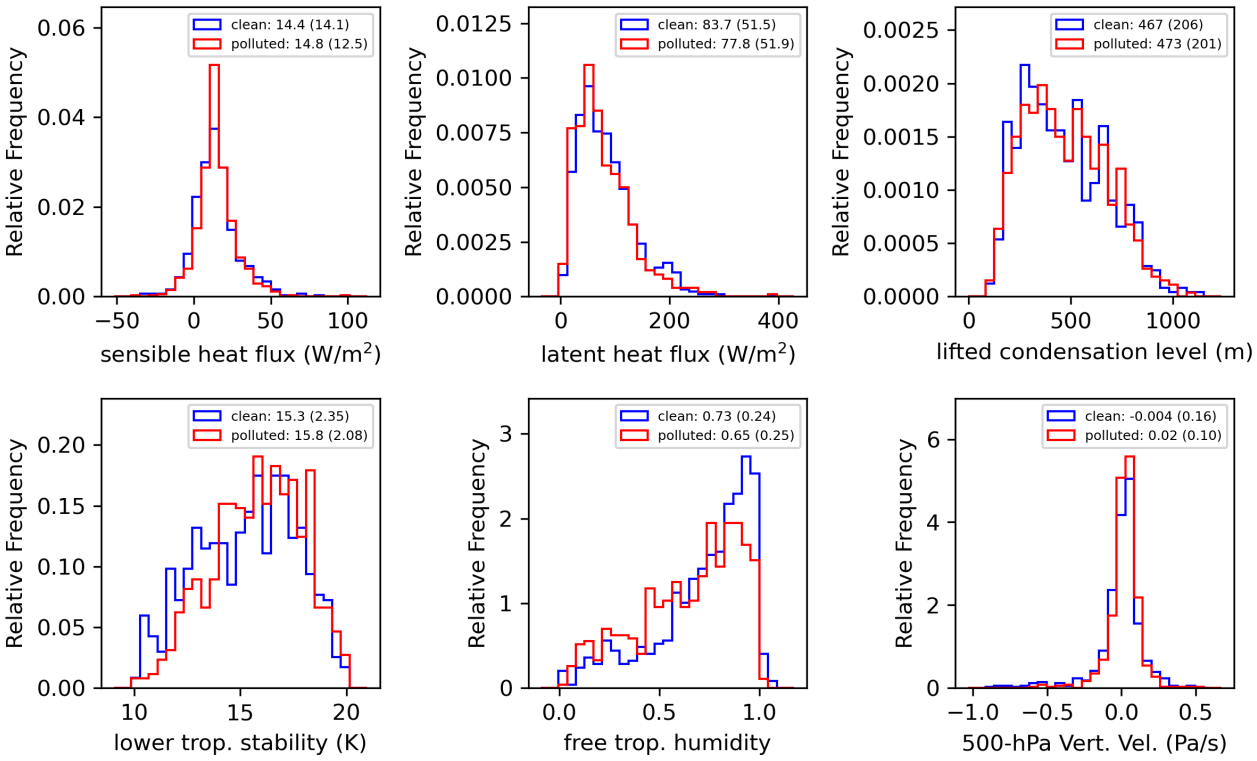

Figure S10. Histograms of cloud controlling meteorological variables: (a) surface sensible heat flux, (b) surface latent heat flux, (c) lifted condensation level, (d) lower tropospheric static stability, (e) free tropospheric humidity, and (e) free-troposheric subsidence rate at 500 hPa at the ENA site at the intial time of the trajectory sorted by below-median (clean; blue) and and above-meddian(polluted; red) CCN concentration.

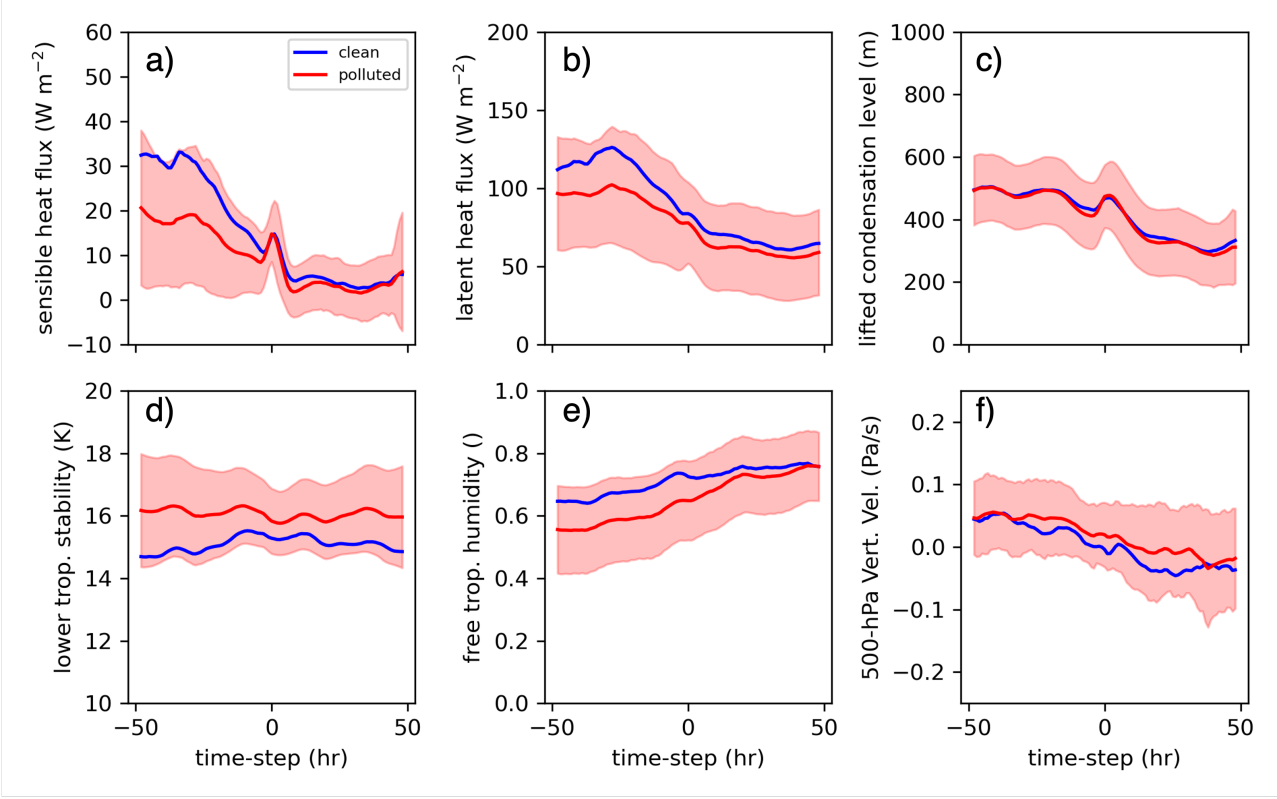

Figure S11. Time-series of cloud controlling meteorological variables: (a) surface sensible heat flux, (b) surface latent heat flux, (c) lifted condensation level, (d) lower tropospheric static stability, (e) free tropospheric humidity, and (e) free-troposheric subsidence rate at 500 hPa of trajectories passing through the ENA site sorted by below-median (clean; blue) and and above-meddian(polluted; red) CCN concentration. Pink envelops denote the 5-95 % confidence interval.

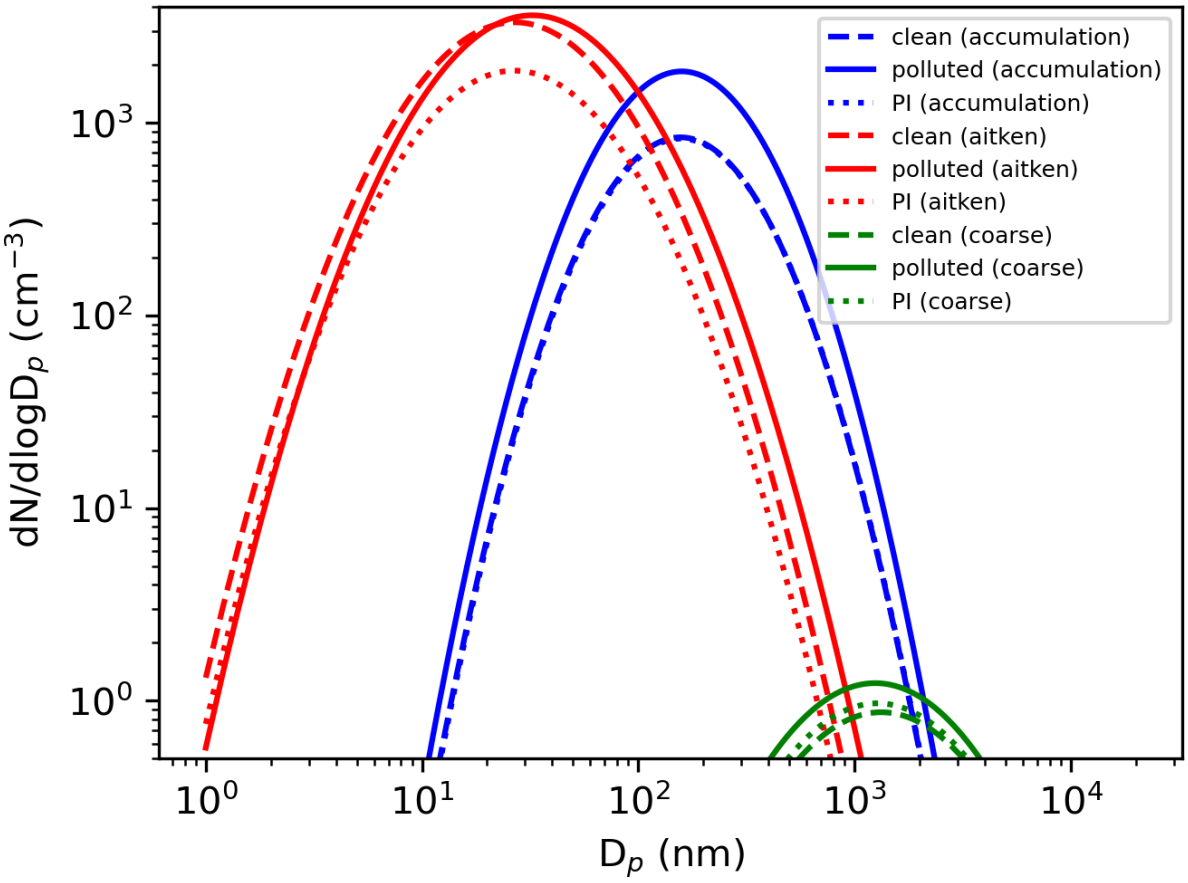

Figure S12. Lognormal aerosol size distribution for interstitial aerosols modeled by MAM4 using total column number, mean aerosol radius, and fixed sigma values for accumulation (blue), Aitken (red), and coarse (green) modes for present day clean (dashed), polluted (solid), and pre-industrial (dotted) conditions.

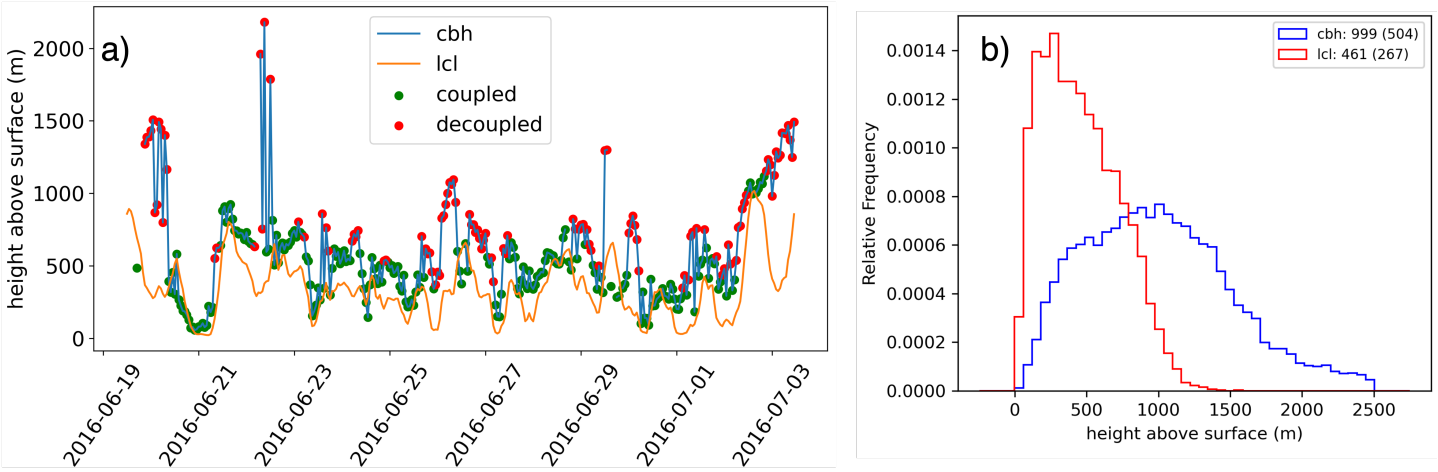

Figure S13. (a) Cloud base height (cbh; blue) retrieved from the ceiliometer, lifted condensation level (lcl; orange) computed from the surface temperature and humidity at noon local time, and clouds which are coupled (green) and decoupled (red) based on a difference in height less than or greater than 300 m, respectively over a two-week period at the ARM ENA site. (b) Histogram of the LCL and CBH at noon local time over the period 08/21/2016 – 08/29/2020.

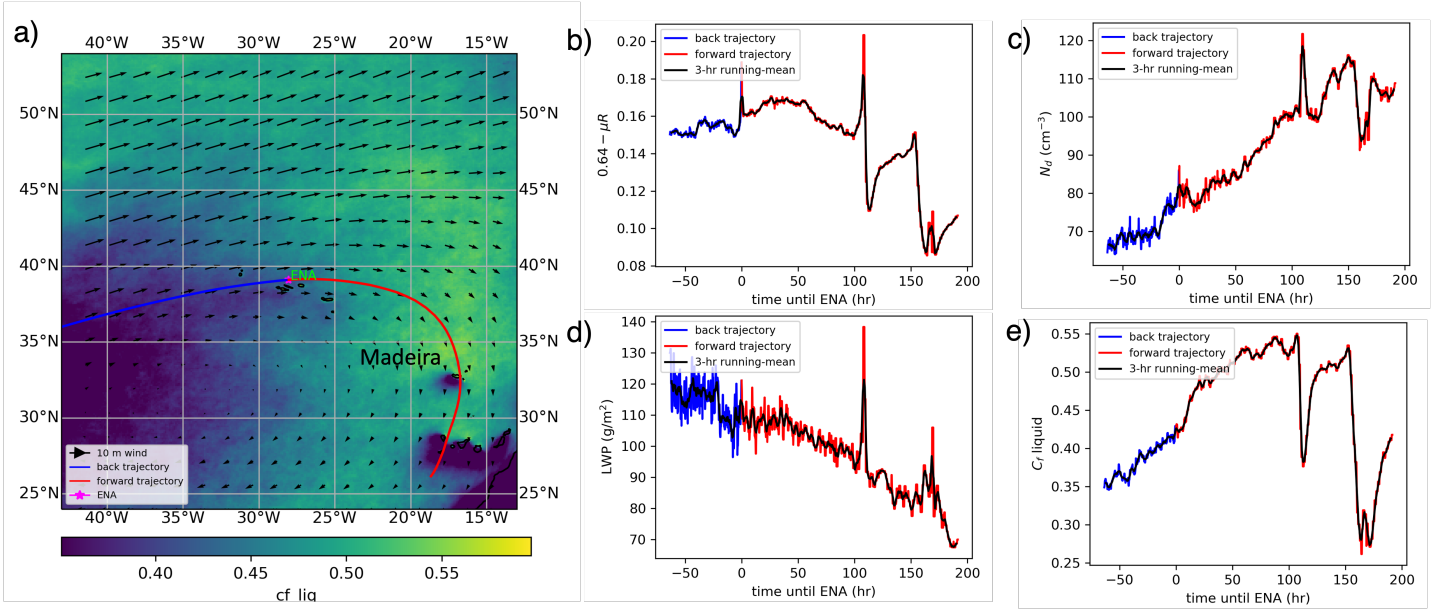

Figure S14. (a) Average cloud fraction for liquid clouds as retrieved using the MODIS instrument on satellites Terra and Aqua and 10-m winds extracted from the MERRA2 reanalysis product for the period 08/21/2016 – 08/29/2020. An back (blue) and forward (red) trajectories based on the mean-state wind-field are calculated from the ENA site. Time-series along the trajectories of the (b) reflectance at $0.64-\mu$m, (c) cloud droplet number concentration, (d) liquid water path, and (e) liquid cloud fraction is averaged over this period. The location of Madeira island is provided for reference.

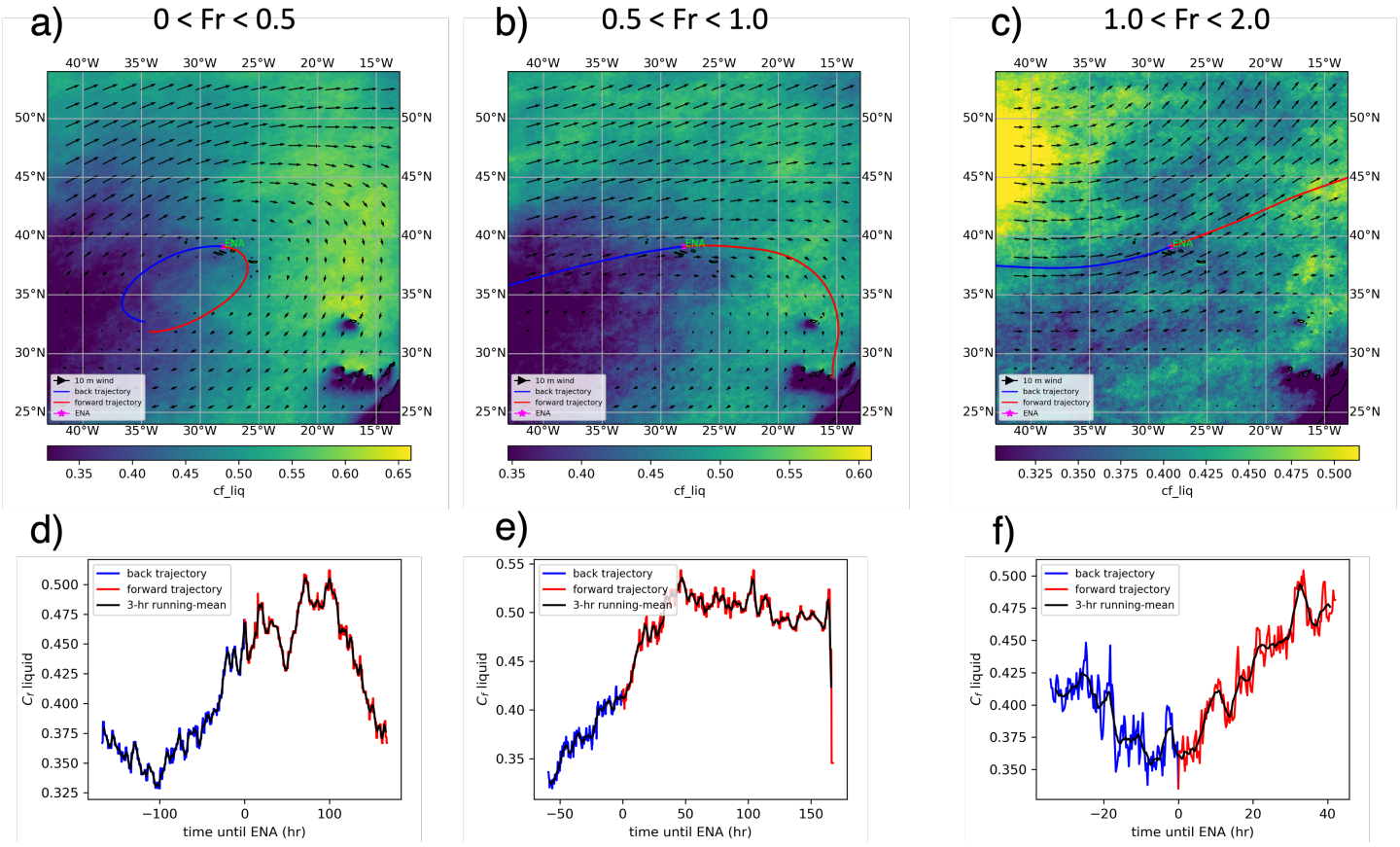

Figure S15. (a) Average cloud fraction for liquid clouds as retrieved using the MODIS instrument on satellites Terra and Aqua and 10-m winds extracted from the MERRA2 reanalysis product for the period 08/21/2016 – 08/29/2020 for Froude numbers between (a) 0 and 0.5, (b) 0.5 and 1.0, and (c) 1.0 and 2.0. Time-series of the mean liquid cloud fraction is provided along the trajectories for each Froude number composite (d,e,f), respectively.

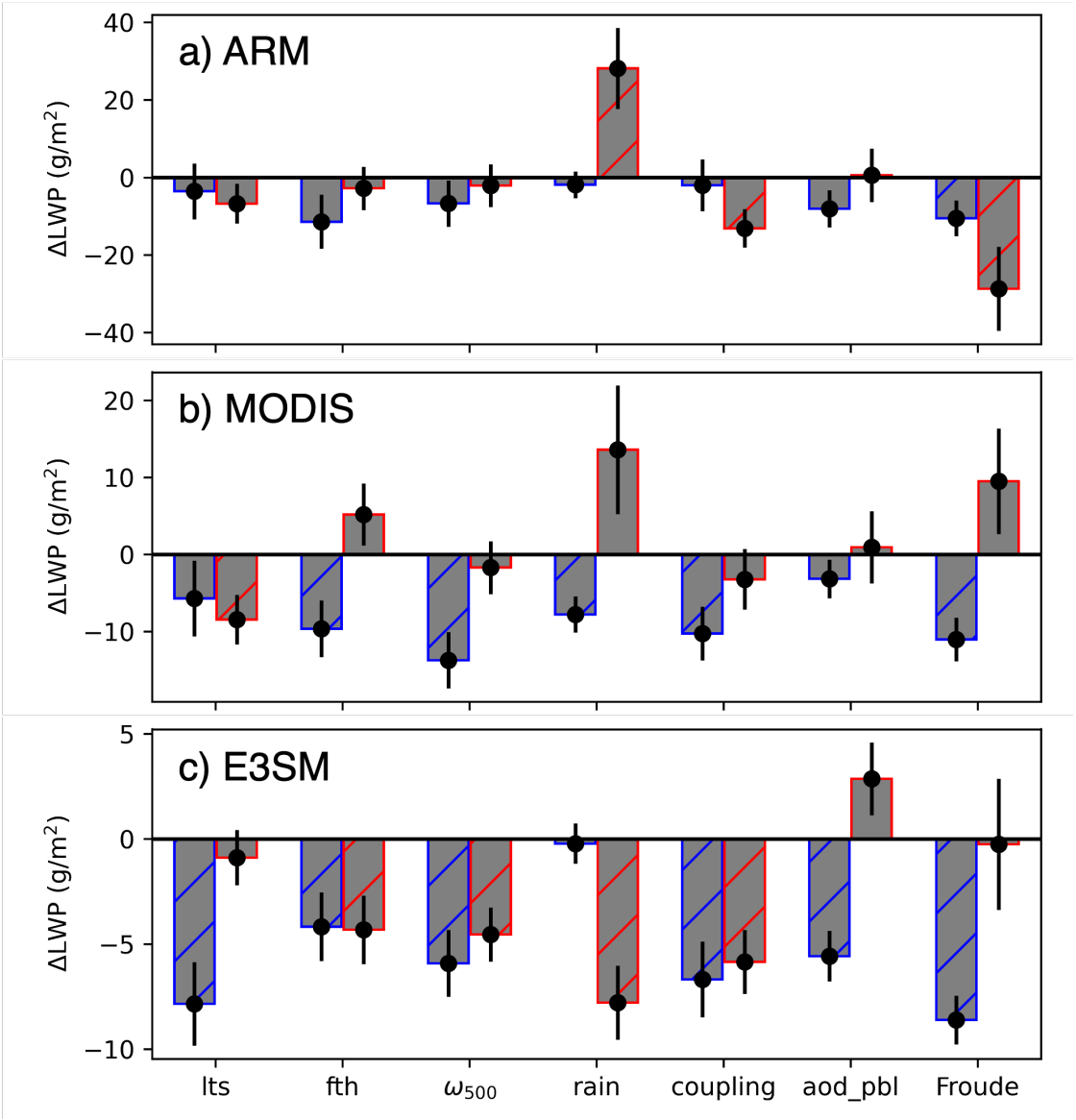

Figure S16. Difference in liquid water path (ΔLWP) between polluted (CCN > 110 cm^{-3}) and clean (CCN < 110 cm^{-3}) trajectories within 6 hours of the CCN observation for (a) ARM, (b) MODIS, and (c) E3SM. Data are stratified by below (blue) and above (red) median lower tropospheric stability (LTS), free-tropospheric humidity (FTH), vertical velocity at 500-hPa (ω_500), rain rate (non-raining and raining), coupling strength (coupled, non-coupled), amount of aerosol in the PBL (aod_pbl) and by Froude number (values 0–1 and 1–2). Error bars represent the 95% confidence interval computed from a two-tailed t-test. Hatching denotes statistically significant differences.

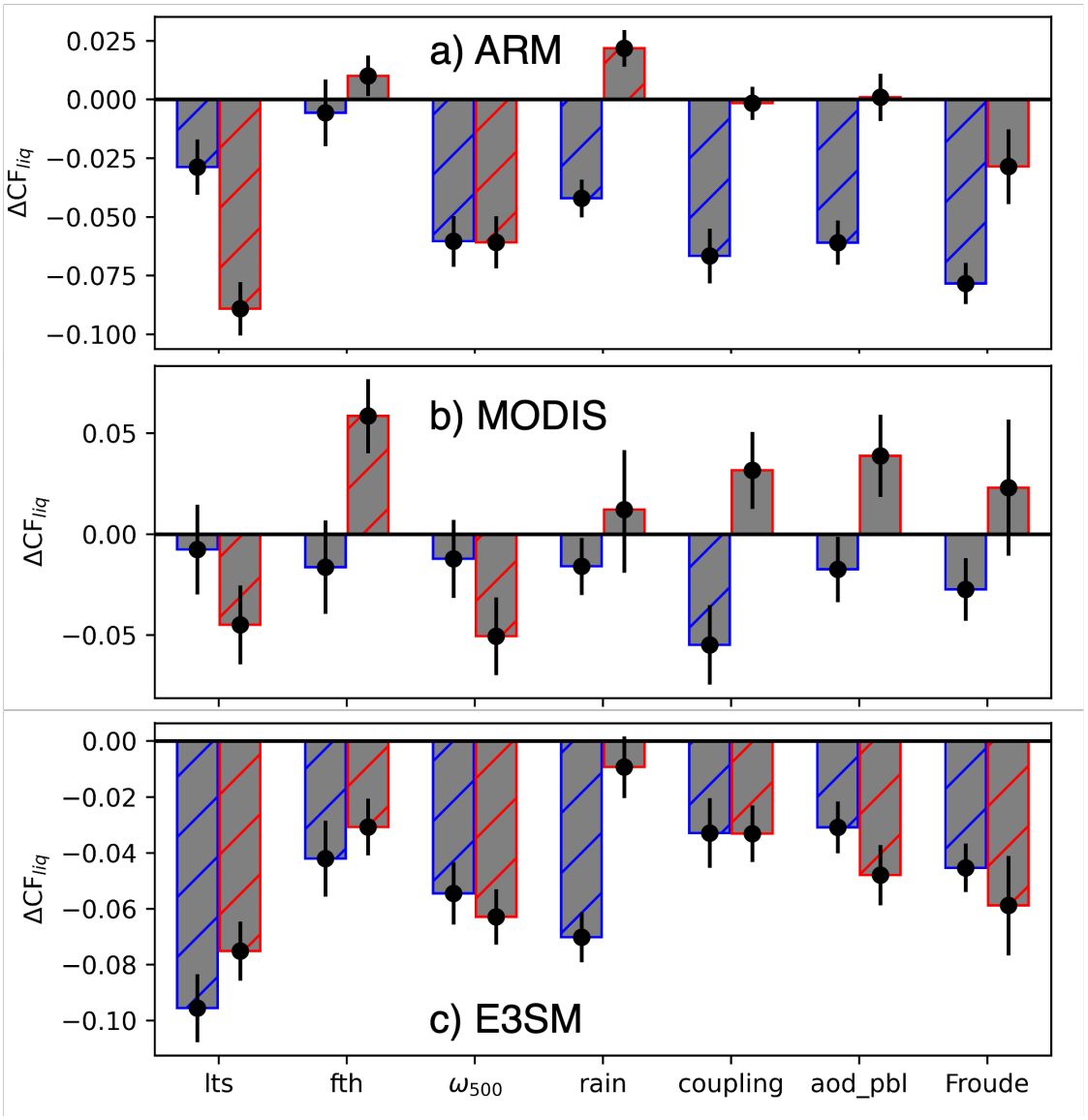

Figure S17. Difference in low-level liquid cloud fraciton (ΔCF_{liq}) between polluted (CCN > 110 cm^{-3}) and clean (CCN < 110 cm^{-3}) trajectories within 6 hours of the CCN observation for (a) ARM, (b) MODIS, and (c) E3SM. Data are stratified by below (blue) and above (red) median lower tropospheric stability (LTS), free-tropospheric humidity (FTH), vertical velocity at 500-hPa (ω_500), rain rate (non-raining and raining), coupling strength (coupled, non-coupled), amount of aerosol in the PBL (aod_pbl) and by Froude number (values 0–1 and 1–2). Error bars represent the 95% confidence interval computed from a two-tailed t-test. Hatching denotes statistically significant differences.

Table S1. Difference in below-cloud and in-cloud wet scavenging rates between different autoconversion experiments (A0R0, A1R0). Bolden font indicates that the difference is statistically significant at the 95th percentile.

Aerosol mode	(A1R0 − A0R0)/A0R0	(A1R1 − A0R1)/A0R1
Below-cloud Accumulation-mode	-0.03	-0.04
Below-cloud Aitken mode	0.07	-0.03
Below-cloud Coarse mode	-0.03	-0.015
In-cloud Accumulation mode	**0.15**	**0.14**
In-cloud Aitken mode	**0.29**	**0.29**
In-cloud Coarse mode	**0.22**	**0.23**